*magnetochemistry*

MDPI

*Article*

# Electronic Influence of Trifluoromethyl Substituents on Benzoate Ligands in Paddlewheel-Type Diruthenium(II,II) Naphthyridine Complexes

**Nozomi Tada, Natsumi Yano, Makoto Handa * and Yusuke Kataoka ***

Department of Chemistry, Graduate School of Natural Science and Technology, Shimane University, 1060 Nishikawatsu, Matsue 690-8504, Shimane, Japan

* Correspondence: handam@riko.shimane-u.ac.jp (M.H.); kataoka@riko.shimane-u.ac.jp (Y.K.)

## Abstract

Two diruthenium(II,II) naphthyridine complexes coordinated with 4-trifluoromethylbenzoate ($O_2CPh\text{-}4\text{-}CF_3$) and 3,5-bis(trifluoromethyl)benzoate ($O_2CPh\text{-}3,5\text{-}diCF_3$) ligands, formulated as $[Ru_2(npc)_2(O_2CPh\text{-}4\text{-}CF_3)_2]$ (**4**; npc = 1,8-naphthyridine-2-carboxylate) and $[Ru_2(npc)_2(O_2CPh\text{-}3,5\text{-}diCF_3)_2]$ (**5**), respectively, were synthesized and structurally characterized. Single-crystal X-ray diffraction analysis revealed that both **4** and **5** form a direct metal–metal bond between the two Ru ions (2.2893(8) and 2.2896(7) Å, respectively) and adopt a paddlewheel-type structure in which two npc and two trifluoromethyl-substituted benzoate ligands are coordinated to a $Ru_2^{4+}$ core with a *cis*-2:2 arrangement. The temperature dependence of the magnetic susceptibility measurements of **4** and **5** exhibited very large zero-field splitting ($D$ = 242 and 246 $cm^{-1}$, respectively) of the triplet ground state of the $Ru_2^{4+}$ core, similar to that of $[Ru_2(npc)_2(O_2CPh)_2]$ (**3**; $D$ = 238 $cm^{-1}$). Owing to the effects of the trifluoromethyl substituents, compared with **3**, **4** and **5** showed (i) a significant blue shift of the absorption bands in the visible region and (ii) a positive shift of the redox potentials, with both shifts becoming more pronounced as the number of trifluoromethyl substituents increased. These experimental results are in good agreement with the electronic structure results obtained from density functional theory calculations.

**Keywords:** diruthenium complex; paddlewheel-type structure; magnetic properties; electronic structure; crystal structure



Academic Editor: Carlos J. Gómez García

Received: 3 November 2025
Revised: 25 November 2025
Accepted: 25 November 2025
Published: 27 November 2025

**Citation:** Tada, N.; Yano, N.; Handa, M.; Kataoka, Y. Electronic Influence of Trifluoromethyl Substituents on Benzoate Ligands in Paddlewheel-Type Diruthenium(II,II) Naphthyridine Complexes. *Magnetochemistry* **2025**, *11*, 104. https://doi.org/10.3390/magnetochemistry11120104



## 1. Introduction

Paddlewheel-type dinuclear complexes, formulated as $[M_2(BL)_4(AL)_n]$ (M: metal ion, BL: bridging ligand, AL: axial ligand, n = 0–2), are intriguing coordination compounds, not only because of their fundamental interest in the study of metal–metal bonds and electronic structures [1–9], but also because of their rich functionalities arising from the unique *d*-orbital interactions within the $M_2$ core [10–18]. The oxidation states and electronic structures of the $M_2$ core in these types of complexes are influenced by the nature of the BL and AL [1]. In this type of structural motif, diruthenium ($Ru_2$) complexes are especially interesting because (i) they are capable of forming three oxidation states ($Ru_2^{6+}$/$Ru_2^{5+}$/$Ru_2^{4+}$) with an open-shell spin state arising from *d*-orbital interactions within the $Ru_2$ core through proper selection and adjustment of the BL [1,4–6], and (ii) they exhibit intrinsic functional properties, such as magnetism [19–22], catalysis [23–26], metallodrug activity [27,28], and electrochromism [29]. The $Ru_2^{5+}$ complexes are known to be

stable when exposed to oxygen and can be readily handled in air, whereas $Ru_2^{4+}$ complexes are generally unstable when exposed to oxygen and are readily oxidized in air [30,31]. Against this background, we recently developed a 1,8-naphthyridine-2-carboxylate (npc)-bridged $Ru_2^{4+}$ complex, $[Ru_2(npc)_2(O_2CCH_3)_2]$ (**1**; Scheme 1a), which is stable in air in both solid and solution states [32]. Single crystal X-ray diffraction (SCXRD) analysis revealed that **1** adopts a paddlewheel-type structure in which the $Ru_2^{4+}$ core is coordinated by two npc and two acetate ligands in a *cis*-2:2 coordination arrangement. Interestingly, **1** is a redox-active compound (redox potential: $E_{1/2}(Ru_2^{5+/4+})$ = 0.43 V vs. SCE) and possesses strong visible absorption bands (781–552 nm), arising from charge transfer from the $Ru_2$ core to the npc ligands. This absorption feature of **1** is unique and not observed in conventional paddlewheel-type $Ru_2$ complexes bridged by four carboxylate ligands ($O_2CR$), $[Ru_2(O_2CR)_4(AL)_2]$. The two acetate ligands in **1** can be exchanged with other carboxylate ligands, thereby shifting their electrochemical and absorption properties [32–34]. For example, owing to the electron-withdrawing effect of the trifluoromethyl substituents, the $E_{1/2}(Ru_2^{5+/4+})$ value of $[Ru_2(npc)_2(O_2CCF_3)_2]$ (**2**; 0.72 V vs. SCE) is shifted in the positive direction, and the absorption bands are also blue-shifted by approximately 70–100 nm compared with those of **1** [33]. In addition, we confirmed that the absorption and redox potentials of $[Ru_2(npc)_2(O_2CPh)_2]$ (**3**) are slightly shifted relative to those of **1** and that these properties show further pronounced shifts upon extension of the aromatic π-ring in the carboxylate ligands [34].

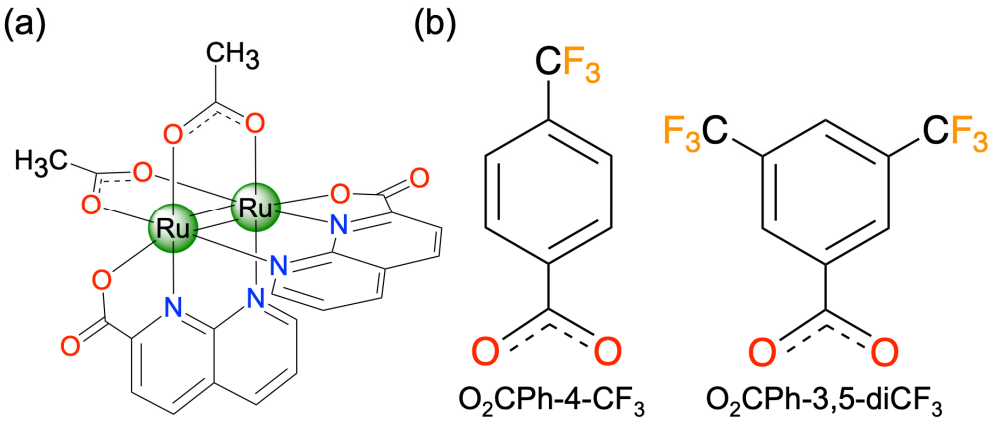


**Scheme 1.** Molecular structures of (**a**) $[Ru_2(npc)_2(O_2CCH_3)_2]$ and (**b**) trifluoromethyl-substituted benzoate ligands used in this study.

It has been reported that the introduction of substituents into the benzoate ligands of homoleptic paddlewheel-type $Ru_2$ complexes enables control of their redox potentials [35–37]. Therefore, we became interested in how the introduction of substituents onto the benzoate ligands of **3** would influence the molecular and electronic structures of $Ru_2$ naphthyridine complexes and how such modifications lead to differences in their characteristic absorption bands and redox potentials. In this study, two $Ru_2$ naphthyridine complexes with trifluoromethyl-substituted benzoate ligands (Scheme 1b), $[Ru_2(npc)_2(O_2CPh\text{-}4\text{-}CF_3)_2]$ (**4**; $O_2CPh\text{-}4\text{-}CF_3$ = 4-trifluoromethylbenzoate) and $[Ru_2(npc)_2(O_2CPh\text{-}3,5\text{-}diCF_3)_2]$ (**5**; $O_2CPh\text{-}3,5\text{-}diCF_3$ = 3,5-bis(trifluoromethyl)benzoate), were synthesized and characterized. The detailed molecular structures of **4** and **5** were determined by SCXRD. Furthermore, the absorption and electrochemical properties as well as the electronic structures of **4** and **5** were closely investigated through a combination of experimental measurements and theoretical calculations and subsequently compared with those of **1**–**3**.

## 2. Materials and Methods

### *2.1. Chemicals and Instruments*

The chemicals used in this study were of reagent or analytical grade and were generally used as received from the suppliers; only tetra-*n*-butylammonium hexafluorophosphate ($TBAPF_6$) was recrystallized from ethanol before use. 4-Trifluoromethylbenzoic acid ($HO_2CPh\text{-}4\text{-}CF_3$) was purchased from Tokyo Chemical Industry Co., Ltd. (Tokyo, Japan), and 3,5-bis(trifluoromethyl)benzoic acid ($HO_2CPh\text{-}3,5\text{-}diCF_3$) was obtained from Matrix Scientific (Elgin, SC, USA), and other chemicals were purchased from Fujifilm Wako Pure Chemical Industry (Osaka, Japan). **1**–**3** were prepared as described previously [32,33].

Proton nuclear magnetic resonance spectroscopy ($^1H$ NMR) was measured using a JEOL (Tokyo, Japan) JNM-ECZR500R spectrometer (500 MHz) in DMSO-$d_6$. The chemical shifts were calibrated using the residual DMSO signal at $\delta$ = 2.49 ppm. Electrospray ionization mass spectrometry (ESI-MS) was performed with a Bruker (Billerica, MA, USA) micrOTOF-II instrument in the positive-ion mode using sodium formate as the calibrant. Elemental analyses of hydrogen, carbon, and nitrogen were performed using a Yanaco CHN Corder MT-6 instrument (Tokyo, Japan). The temperature dependence of the magnetic susceptibility was measured using a Quantum Design (San Diego, CA, USA) MPMS3 SQUID magnetometer under a magnetic field of 5000 Oe over the temperature range of 2–300 K. Cyclic voltammetry (CV) measurements of 1.0 mM **4** and **5** in dried *N*,*N*-dimethylformamide (DMF) solution containing 0.10 M $TBAPF_6$ were performed using a HOKUTO DENKO HZ-7000 HAG1232m system (Tokyo, Japan) equipped with a glassy carbon working electrode, platinum wire counter electrode, and saturated calomel reference electrode (SCE) at a scan rate of 100 mV/s under an Ar atmosphere. Absorption spectrum was recorded in DMF using a JASCO (Tokyo, Japan) UV-670 spectrophotometer.

### *2.2. Synthesis of $[Ru_2(npc)_2(O_2CPh\text{-}4\text{-}CF_3)_2]$ (**4**)*

**1**$(H_2O)_{0.5}$ (67.6 mg, 0.100 mmol) and $HO_2CPh\text{-}4\text{-}CF_3$ (380.2 mg, 2.00 mmol) were dissolved in 15.0 mL of $CH_3OH$, and the mixture was heated at 433 K under Ar for 48 h using a Teflon-lined stainless-steel autoclave reactor. The resulting reaction solution was evaporated, and the crude product was purified by silica gel column chromatography using $CHCl_3/CH_3OH$ (4:1) as the eluent. The dark blue fraction was collected and evaporated to dryness, and resulting dark blue residue was dried under vacuum at 433 K for 3 h. Yield: 82.3 mg (0.0871 mmol, 87.1%). EA calcd (%) for $C_{34}H_{18}N_4O_8F_6Ru_2\cdot(H_2O)$: C 43.23, H 2.13, N 5.93; found C 43.50, H 2.14, N 5.99. $^1H$ NMR (500 MHz, DMSO-$d_6$, $\delta$): 30.40 (d, 2H), 30.29 (d, 2H), 15.98 (s, 4H), 14.96 (d, 2H), 9.55 (d, 4H), −2.39 (d, 2H), –9.96 (bs, 2H). ESI-MS calcd for $C_{34}H_{18}N_4O_8F_6Ru_2Na$ $[M + Na]^+$: 950.9027 $m/z$, found 950.9021 $m/z$.

### *2.3. Synthesis of $[Ru_2(npc)_2(O_2CPh\text{-}3,5\text{-}diCF_3)_2]$ (**5**)*

A synthetic method similar to **4** was applied for the preparation of **5**, but $HO_2CPh\text{-}3,5\text{-}diCF_3$ (516.4 mg, 2.00 mmol) was used instead of $HO_2CPh\text{-}4\text{-}CF_3$. Yield: 88.5 mg (0.0833 mmol, 83.3%). EA calcd (%) for $C_{36}H_{16}N_4O_8F_{12}Ru_2$: C 40.69, H 1.52, N 5.27; found C 41.00, H 1.82, N 5.78. $^1H$ NMR (500 MHz, DMSO-$d_6$, $\delta$): 29.90 (dd, 4H), 16.08 (s, 4H), 15.33 (d, 2H), 11.46 (s, 2H), −2.33(d, 2H), −11.56 (bs, 2H). ESI-MS calcd for $C_{36}H_{16}N_4O_8F_{12}Ru_2Na$ $[M + Na]^+$: 1086.8776 $m/z$, found 1086.8756 $m/z$.

### *2.4. Single Crystal X-Ray Diffraction Analysis*

The SCXRD experiment of **4** was performed using a RIGAKU (Tokyo, Japan) XtaLAB Synergy-S system equipped with a Hypix-6000 detector and graphite-monochromated Cu $K\alpha$ radiation ($\lambda$ = 1.54184 Å) from a microfocus PhotonJet-S source, whereas that of **5** was conducted using a RIGAKU XtaLAB Synergy-R/DW system equipped with a Hypix-6000

detector and graphite-monochromated Cu $K\alpha$ radiation (λ = 1.54184 Å) from a rotating anode PhotonJet-R source.

The crystals were coated with Paratone-N oil and mounted on a goniometer head using MiTeGen (Ithaca, NY, USA) microloops. Diffraction data were collected at 100 K under the $N_2$ steam, and data processing and reduction were executed using CrysAlisPro software version 1.171.43.108a [38]. The initial structures were solved by intrinsic phasing with SHELXT program [39] and subsequently refined by full-matrix least-squares on $F^2$ using SHELXL program [40] in the Olex2 software version 1.5 [41]. Hydrogen atoms were placed in calculated positions and refined as riding models, while all non-hydrogen atoms were refined anisotropically. The crystallographic data for the final refined structures of **4** and **5** are summarized in Table 1 and can be obtained free of charge from Cambridge Crystallographic Data Centre (CCDC). The deposition numbers of **4** and **5** are CCDC-2499389 and 2499390, respectively.

**Table 1.** Crystallographic data of **4** and **5**.

| | **4** | **5** |
|---|---|---|
| Chemical formula | $C_{40}H_{29}F_6N_7O_9Ru_2$ | $C_{36}H_{18}F_{12}N_4O_9Ru_2$ |
| Formula weight | 1067.84 | 1080.68 |
| Crystal system | monoclinic | orthorhombic |
| Space group | $P\ 2_1/c$ | $P\ na2_1$ |
| $a$ [Å] | 14.3266(2) | 22.9594(3) |
| $b$ [Å] | 10.25320(10) | 16.2295(2) |
| $c$ [Å] | 27.8368(3) | 10.00890(10) |
| $\alpha$ [°] | 90 | 90 |
| $\beta$ [°] | 99.0220(10) | 90 |
| $\gamma$ [°] | 90 | 90 |
| $V$ [Å$^3$] | 4038.46(8) | 3729.51(8) |
| Z | 4 | 4 |
| $D_{calc}$(g cm$^{-3}$) | 1.756 | 1.925 |
| μ [mm$^{-1}$] | 6.889 | 7.685 |
| $F$(000) | 2128.0 | 2120.0 |
| $R_1$ ($I > 2\sigma(I)$) | 0.0692 | 0.0368 |
| $wR_2$ ($I > 2\sigma(I)$) | 0.1723 | 0.0970 |
| $R_1$ (all data) | 0.0703 | 0.0369 |
| $wR_2$ (all data) | 0.1727 | 0.0971 |
| GOF on $F^2$ | 1.240 | 1.077 |

### *2.5. Quantum Chemical Calculation Methods*

All quantum chemical calculations in this study were performed using the spin-unrestricted density functional theory (DFT) functional B3LYP [42], in combination with the SDD basis set for Ru atoms [43], the aug-cc-pVDZ basis set for N and O atoms, and the cc-pVDZ basis set for other atoms [44], as implemented in the Gaussian 16 (Rev. C.01) program suite [45]. Molecular geometries were fully optimized without symmetry constraints, and the obtained geometries were verified as minima using frequency analysis. The solvent effect of DMF ($\varepsilon$ = 37.219) was considered by employing the polarizable continuum model [46]. Time-dependent DFT (TDDFT) calculations were performed to investigate the characteristics of vertical excitations from the ground state [47].

## 3. Results

### *3.1. Synthesis and Characterization*

Complexes **4** and **5** were synthesized via ligand-exchange reactions at 433 K between complex **1** and 20 equivalents of $HO_2$CPh-4-$CF_3$ and $HO_2$CPh-3,5-di$CF_3$, respectively,

under solvothermal conditions in an Ar atmosphere. Dark blue powders of **4** and **5** were obtained in 87.1 and 83.3% yields, respectively. Although the reaction was attempted under reflux conditions, the reaction did not procced sufficiently. The obtained **4** and **5** were paramagnetic compounds and stable both in the solid solution states in air.

Complexes **4** and **5** were characterized using paramagnetic $^1$H NMR, ESI-MS, and CHN elemental analyses. In the $^1$H NMR spectra (Figures S1 and S2), the signals assignable to the two npc ligands of **4** appear at 30.40, 30.29, 14.96, −2.39, and −9.96 ppm with an integral ratio of 2:2:2:2:2, whereas those of **5** appear at 29.90, 15.33, −2.33, and −11.56 ppm with an integral ratio of 4:2:2:2; the most downfield signal of **5** is a doublet of doublets. In addition, proton signals with total integral ratios of 8 and 6 derived from the two $O_2$CPh-4-$CF_3$ ligands in **4** (15.98, 9.55 ppm) and two $HO_2$CPh-3,5-di$CF_3$ ligands in **5** (16.08, 11.46 ppm) were also observed. The ESI-MS spectra of **4** and **5** show intense peaks at 950.9021 and 1086.8756 $m/z$, respectively, which are in good agreement with the [M + Na]$^+$ values (950.9027 and 1086.8776 $m/z$, respectively) corresponding to the molecular formulas composed of two Ru ions, two npc ligands, and two $O_2$CPh-4-$CF_3$ or $O_2$CPh-3,5-di$CF_3$ ligands, respectively (Figures S3 and S4). The $^1$H NMR and ESI-MS results, as well as the elemental analysis, strongly indicate that **4** and **5** adopt structures with the chemical formula [$Ru_2$(npc)$_2$($O_2$CR)$_2$], similar to those of **1**–**3**.

### *3.2. Crystal Structures*

Single crystals of **4** and **5** suitable for SCXRD measurements were obtained by the slow evaporation of mixed $CH_3$CN/DMSO solutions containing **4** and **5**, respectively. Diffraction analyses revealed that **4** crystallizes in a monoclinic system with the $P\,2_1/c$ space group, whereas **5** crystallizes in an orthorhombic system with the $P\,na2_1$ space group. The final refined crystal structures of **4** and **5** with the selected numbering schemes are shown in Figure 1, and their selected structural parameters (bond lengths and angles) are summarized in Tables S1 and S2, respectively.

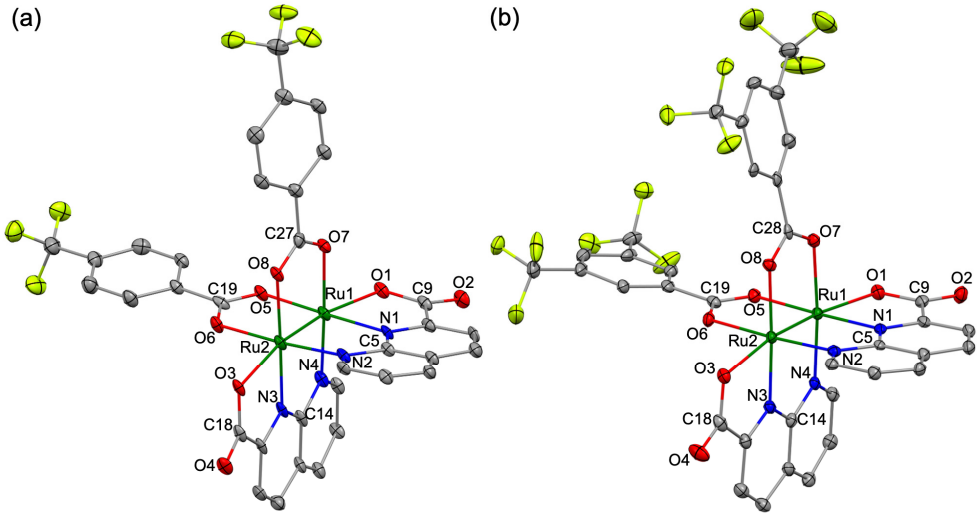


**Figure 1.** Crystal structures of (**a**) **4** and (**b**) **5**. Thermal ellipsoids were represented at a 30% probability level. Hydrogen atoms and solvents were omitted for clarity.

Structural analysis revealed that the asymmetric units of both **4** and **5** comprised one crystallographically independent molecule of [$Ru_2$(npc)$_2$($O_2$CR)$_2$], together with co-crystallized solvent molecules (for **4**: three $CH_3$CN and one $H_2O$; for **5**: one $H_2O$). The final refined crystal structures of **4** and **5** adopted a paddlewheel-type structure, in which the $Ru_2^{4+}$ core was coordinated by two npc and two trifluoromethyl-substituted benzoate ligands in a *cis*-2:2 coordination arrangement, similar to those of **1**–**3** [32,33].

The Ru–Ru bond lengths of **4** and **5** were estimated to be 2.2893(8) and 2.2896(7) Å, respectively, which show no significant differences from those of **1** (2.2893(4) Å), **2** (2.2978(4) Å), **3** (2.2834(6) Å), and other $Ru_2^{4+}$ complexes such as $[Ru_2(O_2CCH_3)_4(H_2O)_2]$ (2.262(3) Å) [30] and $[Ru_2(pynp)_2(O_2CCH_3)_2](PF_6)_2$ (2.298(1) Å; pynp = 2-(2-pyridyl)-1,8-naphthyridine) [48], indicating the formation of a double bond between two Ru ions in **4** and **5**. The two npc ligands of **4** and **5** were coordinated to the $Ru_2$ core in a tridentate fashion; specifically, the naphthyridine and carboxylate moieties of each npc ligand were coordinated to the equatorial and axial positions of the $Ru_2$ core, respectively. The average Ru–N(npc)/Ru–O(npc) bond lengths of **4** and **5** were 2.060/2.238 Å and 2.058/2.213 Å, respectively, with no significant difference between them. Two trifluoromethyl-substituted benzoate ligands bound to the $Ru_2$ core in a syn–syn μ-bridging coordination mode [49]; the averaged Ru–O(μ-carboxylate) bond lengths of **4** and **5** were both 2.078 Å. The bond lengths in these primary coordination spheres differed by less than 0.01 Å from those of **3** [32]. Therefore, the influence of introducing trifluoromethyl substituents into the benzoate ligands of the $[Ru_2(npc)_2(O_2CR)_2]$ complex on the Ru–Ru bond length and the bond lengths in the primary coordination sphere was negligibly small.

The two npc ligands coordinated in a coplanar manner to the $Ru_2$ core, whereas the two trifluoromethyl-substituted benzoate ligands coordinated in a tilted manner, and their phenyl and carboxylate planes were slightly twisted (average rotation angles: 7.27° for **4** and 7.87° for **5**). These distortions were not caused by the trifluoromethyl-substituents because the optimized structures of **4** and **5** obtained from DFT calculations (described later) did not show such tilting or twisting. In the packing structures of **4** and **5**, the crystallization water molecules formed hydrogen bonds with the carboxylate moieties of the npc ligands, giving rise to a one-dimensional hydrogen-bonding network (see Figures S5 and S6).

### *3.3. Magnetic Susceptibilities*

To investigate the magnetic properties as well as the electronic spins and oxidation states of **4** and **5**, the temperature dependence of the magnetic susceptibilities were measured using a SQUID magnetometer under an applied field of 5000 Oe over a temperature range of 2–300 K. The effective magnetic moments of **4** and **5** at 300 K were estimated to be 2.90 and 2.87 $\mu_B$, respectively; these values are close to the spin-only value of 2.83 $\mu_B$ for the triplet spin state of the $Ru_2^{4+}$ complex but deviate significantly from the 3.87 $\mu_B$ expected for the quartet spin ($S = 3/2$) state of the $Ru_2^{5+}$ complex. Figure 2 shows the temperature dependence of the molar magnetic susceptibility ($\chi_M$) and effective moments ($\mu_{eff}$) of **4** and **5**. Similar to **1**–**3** [32,33], the $\mu_{eff}$ values decreased with decreasing temperature. At 2 K, the $\mu_{eff}$ values of **4** and **5** reached 0.38 and 0.35 $\mu_B$, respectively. This temperature-dependent behavior can be ascribed to the zero-field splitting (ZFS) characteristics of the $Ru_2$ complexes [50–52].

To elucidate the ZFS characteristics of **4** and **5** in detail, their $D$ tensors and $g$ values were determined by fitting the measured data to Equation (1) [32–34].

$$\chi_M = (1-\rho)\left[\frac{2N\beta^2 g^2}{3kT}\cdot\frac{\left\{e^{-\frac{D}{kT}}+\left(\frac{2kT}{D}\right)\left(1-e^{-\frac{D}{kT}}\right)\right\}}{\left(1+2e^{-\frac{D}{kT}}\right)}\right]+\rho\left(\frac{5N{g_{imp}}^2\beta^2}{4kT}\right) \quad (1)$$

where $\rho$ is the correction term for a small amount of paramagnetic impurities with $S = 3/2$ (0.003 for **4**, 0.001 for **5**), $k$ is the Boltzmann constant, $N$ is Avogadro's number, $\beta$ is the Bohr magneton, and the $g_{imp}$ value is assumed to be equal to the $g$ value. The fitting results were as follows: (i) the calculated g values of both **4** and **5** were 2.12, similar to those of **1**–**3** ($g$ = 2.03–2.13) and (ii) the $D$ tensors of **4** and **5** were estimated to be 242 and 246 $cm^{-1}$, respectively. These large $D$ tensor magnitudes are characteristic of $Ru_2^{4+}$ complexes [53,54],

including **1** (227 $cm^{-1}$), **2** (243 $cm^{-1}$), and **3** (238 $cm^{-1}$) [32–34], and significantly larger than those of $Ru_2^{5+}$ complexes such as $[Ru_2(O_2CCH_3)_4(H_2O)_2]BPh_4$ (71.8 $cm^{-1}$) [55]. These results provide strong evidence that **4** and **5** possess a $Ru_2^{4+}$ core with $S = 1$ and that the effects of the trifluoromethyl substituents on their magnetic properties are negligible.

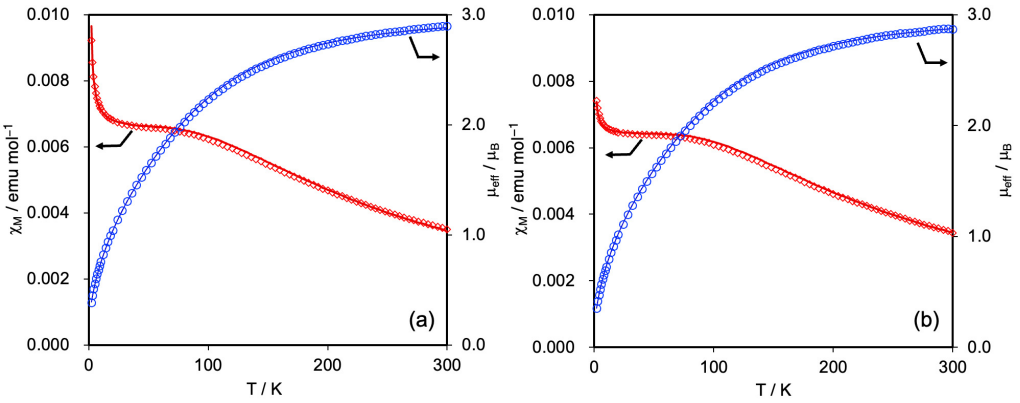


**Figure 2.** Temperature dependence of the magnetic susceptibility (red circle) and effective magnetic moment (blue rhombus) of (**a**) **4** and (**b**) **5**. The solid lines represent the best fit of the data using Equation (1).

### *3.4. Optimized Geometries, Spin Density Distributions, and Electronic Structures*

DFT calculations were performed to investigate the molecular geometries, spin density distributions, and electronic structures of **4** and **5** in detail, and the results were compared with those of **3** [32]. The optimized geometries of **4** and **5** adopted a paddlewheel-type structure, in which two npc and two trifluoromethyl-substituted benzoate ligands were coordinated to the $Ru_2$ core in a *cis*-2:2 arrangement, similar to their crystal structures. The Ru–Ru bond lengths of optimized geometries of **4** and **5** were calculated to be 2.321 and 2.324 Å, respectively. These bond lengths are almost identical to that of 3 (2.318 Å), indicating that the effect of introducing trifluoromethyl substituents into the benzoate ligands on the Ru–Ru bond length is negligibly small. The Ru–Ru bond lengths and the bond lengths between the $Ru_2$ core and the first coordination sphere in **3**–**5** show excellent agreement with those obtained from SCXRD data, with the differences being within 0.035 Å. The trifluoromethyl-substituted benzoate ligands in the optimized geometries of **4** and **5** were coordinated to the $Ru_2$ core without twisting or bending, as observed in **3** [32].

To clarify the origins of the magnetic spins of **4** and **5**, their spin density distributions were estimated. As depicted in Figure 3, the spin density of **4** and **5** are predominantly localized on the $Ru_2$ core (**4**: +2.043, **5**: +2.037) rather than on the npc (**4**: −0.014, **5**: −0.005) and trifluoromethyl-substituted benzoate ligands (**4**: −0.029, **5**: −0.032), which is consistent with the magnetic susceptibility results.

Selected molecular orbital (MO) diagrams and frontier MO pictures, i.e., the highest occupied MO (HOMO) and lowest unoccupied MO (LUMO), of **3**–**5** are shown in Figure 4, where the MOs are separated into α and β spins due to the use of the unrestricted DFT approach. The calculated trends and energy ordering of the MOs for **4** and **5** closely resembled those of **3**. Two singly occupied MOs, i.e., HOMO(α) and HOMO–1(α), of **4** and **5** were both predominantly localized on the π*($Ru_2$) orbitals, as observed in **3**. The δ*($Ru_2$) orbital pairs of **4** and **5** are found at HOMO–2(α) and HOMO(β), whose energies were lower and higher, respectively, than those of the π*($Ru_2$) orbitals (HOMO(α)/HOMO–1(α)). The introduction of trifluoromethyl substituents into the benzoate ligands led to a significant stabilization of the occupied MOs. Specifically, the energies of HOMO(α)/HOMO(β) in **4** and **5** were stabilized by −0.06/−0.08 and −0.10/−0.14 eV, respectively, relative to those in **3**, indicating that the MO stabilization increased with the number of trifluoromethyl

substituents. The LUMO(α, β) and LUMO+1(α) of **4** and **5** were both mainly localized on the π*(npc) orbitals, as observed for **3**. On the other hand, the LUMO+1(β) was primarily composed of the π*($Ru_2$) orbital with a minor contribution from π*(npc) orbital, whereas the LUMO+2(β) mainly consists of π*(npc) orbital with a small *d**($Ru_2$) orbital contribution. In addition, the LUMO+3(β) is predominantly localized on the π*($Ru_2$) orbital. The energies of the unoccupied MOs of **4** and **5** were slightly stabilized by the trifluoromethyl substituents relative to those of **3**, although the stabilization was less pronounced than for the occupied MOs. The energies of LUMO(α)/LUMO(β) in **4** and **5** were stabilized by −0.03/−0.06 and −0.06/−0.05 eV, respectively, relative to those in **3**. The electronic configurations of the $Ru_2$ core in **4** and **5** are $\pi^4\delta^2\sigma^2\delta^{*2}\pi^{*2}$, which are similar to those of **1**–**3**, indicating the formation of a double bond between the two Ru ions in **4** and **5**.

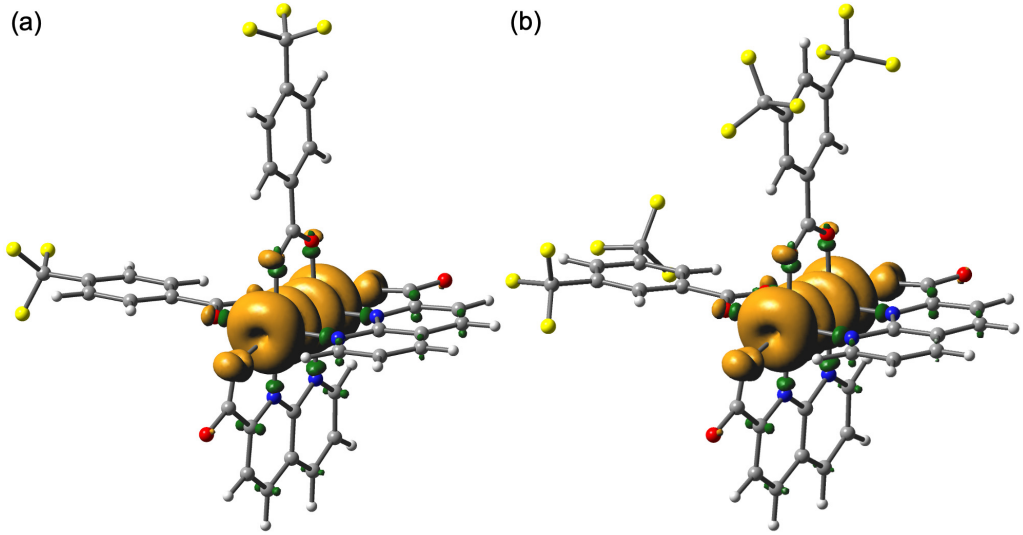


**Figure 3.** Spin density distributions of (**a**) **4** and (**b**) **5** (isovalue = 0.002).

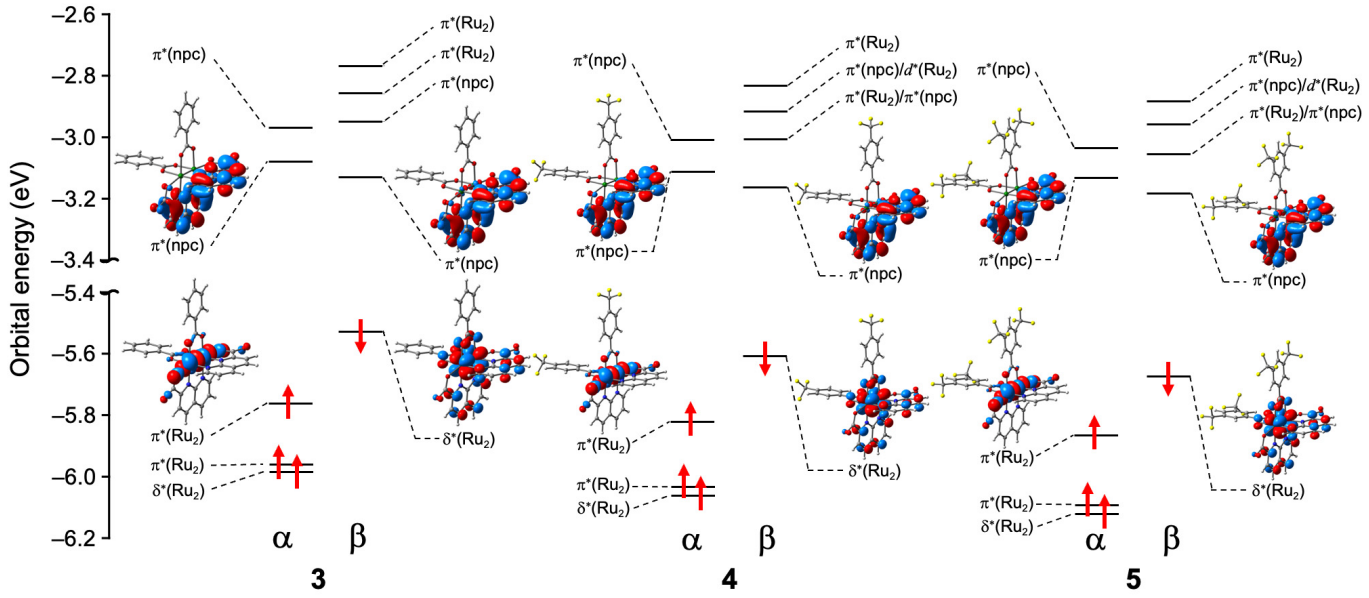


**Figure 4.** MO diagrams and frontier MO pictures of **3**–**5**.

### *3.5. Electrochemical Properties*

To investigate the electrochemical properties of **4** and **5**, cyclic voltammetry (CV) measurements were performed in DMF containing 0.10 M $TBAPF_6$ over the potential range from 1.0 V to −1.8 V vs. SCE. The observed redox potentials ($E_{1/2}$) and the peak separations of the reduction and oxidation waves ($\Delta E$) of **4** and **5** as well as of those of **1**–**3** are summarized in Table 2. As shown in Figure 5, the CV diagrams of **4** and **5** both exhibit one and two reversible waves in the positive and negative regions, respectively, similar to those of **1**–**3** [32–34]. The $E_{1/2}$ values of the waves in the positive region for **4** and **5**, which can be assigned to the $Ru_2^{5+/4+}$ redox couple, were observed at 0.56 and 0.58 V, respectively, and these values were slightly shifted in the positive direction compared with that of **3** (0.52 V). In addition, the $E_{1/2}$ values of the two waves in the negative region for **4** and **5**, attributed to the reduction of npc ligands, were −0.80/−1.15 V and −0.76/−1.12 V, respectively, showing a slight positive shift compared with those of **3** (−0.83/−1.19 V). All $E_{1/2}$ values for **5** appeared at more positive potentials than those for **4**. That is, the slight shifts in the $E_{1/2}$ values can be attributed to the electron-withdrawing effect of the trifluoromethyl substituents. These CV results were consistent with the DFT-calculated electronic structures, in which both the HOMO and LUMO energy levels stabilized as the number of trifluoromethyl substituents increased. The $E_{1/2}$ value of **2** shifted significantly to more positive potentials (~0.29 V) compared with those of **1**. This indicates that a bridging ligand in which an electron-withdrawing group is directly connected to the carboxylate moiety, such as trifluoroacetate, has a greater influence on the $E_{1/2}$ value of the $Ru_2$ naphthyridine complex than bridging ligands in which similar substituents are introduced onto the benzoate ring, even at multiple positions.

**Table 2.** Redox potentials and their separation ($\Delta E$: mV) of **1**–**5**.

| Complex | $E_{1/2}$: V vs. SCE ($\Delta E$: mV) |
|---|---|
| **1** | 0.43 (62), −0.92 (64), −1.19 (64) |
| **2** | 0.72 (68), −0.67 (63), −1.10 (56) |
| **3** | 0.52 (66), −0.83 (56), −1.19 (57) |
| **4** | 0.56 (72), −0.80 (63), −1.15 (64) |
| **5** | 0.58 (67), −0.76 (64), −1.12 (64) |

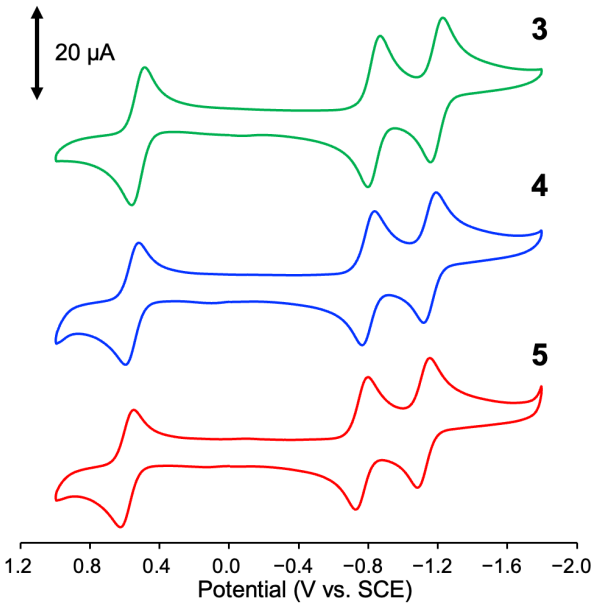


**Figure 5.** CV diagrams of **3** (green), **4** (blue), and **5** (red) in degassed DMF/$TBAPF_6$ (scan rate: 100 mV/s).

### 3.6. Absorption Properties

Figure 6 shows the absorption spectra of **3**–**5** in DMF, and the wavelengths of the absorption maxima and molar absorption coefficients ($\varepsilon$) of **1**–**5** are summarized in Table 3. The lowest-energy absorption bands of **4** and **5**, which were assigned to metal-to-ligand charge transfer (MLCT) transitions from the $Ru_2$ core to the npc ligands, appeared at 736 ($\varepsilon$ = 4135 $M^{-1}$ $cm^{-1}$) and 717 nm ($\varepsilon$ = 4103 $M^{-1}$ $cm^{-1}$), respectively, and were apparently blue-shifted relative to the corresponding band of **3** (771 nm) [32]. The most intense absorption bands of **4** and **5** in the visible region were observed at 598 ($\varepsilon$ = 6352 $M^{-1}$ $cm^{-1}$) and 586 nm ($\varepsilon$ = 6424 $M^{-1}$ $cm^{-1}$), respectively, and intense shoulder bands were discernible at slightly higher energies, centered at 540 and 531 nm, respectively. These bands were also assigned to the MLCT transitions from the $Ru_2$ core to the npc ligands according to TDDFT calculations (Tables S3 and S4). Based on these results, the absorption bands of **4** and **5** were clearly blue-shifted as the number of electron-withdrawing trifluoromethyl substituents on the benzoate increased. However, the energy differences in the absorption bands between **3** and **4** (or **5**) were clearly smaller than those observed between **1** and **2** [32,33].

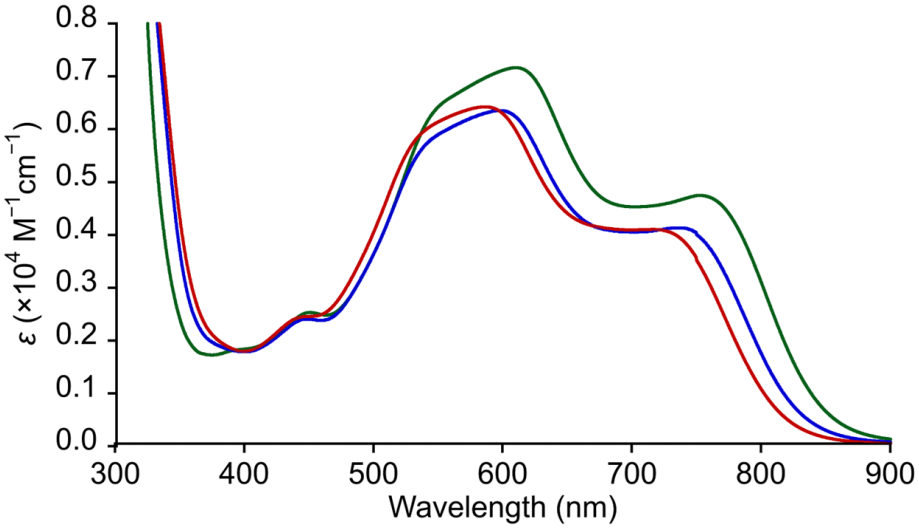


**Figure 6.** Absorption spectra of **3** (green), **4** (blue), and **5** (red) in DMF.

**Table 3.** Absorption wavelengths (nm) and their molar absorption coefficients ($\varepsilon$) of **1**–**5** in DMF.

| Complex | Wavelengths (nm) [$\varepsilon$ ($M^{-1}$ $cm^{-1}$)] |
|---|---|
| **1** | 781 (4313), 621 (6421), 552 (5245) |
| **2** | 686 (3780) *, 555 (6599), 514 (6090) * |
| **3** | 771 (4528), 620 (7164), 548 (6374) |
| **4** | 736 (4135), 598 (6352), 540 (5683) |
| **5** | 717 (4103), 586 (6424), 531 (5760) |

* Shoulder band.

## 4. Conclusions

In summary, we successfully synthesized two paddlewheel-type $Ru_2$ naphthyridine complexes, [$Ru_2$(npc)$_2$($O_2$CPh-4-$CF_3$)$_2$] (**4**; npc = 1,8-naphthyridine-2-carboxylate) and [$Ru_2$(npc)$_2$ ($O_2$CPh-3,5-di$CF_3$)$_2$] (**5**), in which two npc and two trifluoromethyl-substituted benzoate ligands are coordinated to a $Ru_2^{4+}$ core with a *cis*-2:2 arrangement. Direct Ru–Ru bonds were confirmed from the SCXRD results, and a very large zero-field splitting ($D$ = 242 $cm^{-1}$ for **4**, 246 $cm^{-1}$ for **5**) associated with the triplet ground state $Ru_2^{4+}$ core was also observed from magnetic susceptibility measurements, with all these findings further supported by DFT calculations. The obvious effects of the trifluoromethyl substituents

on the benzoate ligands of the $Ru_2$ complexes were confirmed from the absorption and electrochemical properties as well as from the MO energies obtained by DFT calculations. In the electrochemical analysis, compared with that of **3**, the observed redox potentials of **4** and **5** were slightly shifted to more positive values with an increasing number of trifluoromethyl substituents on the benzoate ligands; the $E_{1/2}(Ru_2{}^{5+/4+})$ values of **3**–**5** were 0.52, 0.56, and 0.58 V vs. SCE, respectively. The low-energy absorption bands of **4** and **5** also showed a clear blue shift compared with those of **3**. These shifts are consistent with the DFT calculation results, indicating that the introduction of trifluoromethyl substituents into the benzoate ligands stabilizes the MOs, particularly the occupied orbitals. The differences in the absorption and redox potentials among **3**–**5** were smaller than those observed between **1** and **2**, suggesting that the direct introduction of trifluoromethyl substituents onto the carboxylate, as in trifluoroacetate, exerts a stronger electron-withdrawing effect on the absorption, redox potentials, and electronic structures of the $Ru_2$ naphthyridine complexes than multiple trifluoromethyl substituents on the benzoate ligands.

**Supplementary Materials:** The following supporting information can be downloaded at: https://www.mdpi.com/article/10.3390/magnetochemistry11120104/s1, Figure S1: 1H NMR spectrum of **4** in DMSO-$d_6$; Figure S2: 1H NMR spectrum of **5** in DMSO-$d_6$; Figure S3: Observed and simulated ESI-MS spectra of **4**; Figure S4: Observed and simulated ESI-MS spectra of **5**; Figure S5: One-dimensional hydrogen-bonding network structure of **4** along the *a*-axis; Figure S6: One-dimensional hydrogen-bonding network structure of **5** along the *b*-axis; Table S1: Selected bond lengths (Å) and angles (°) of crystal structure of **4**; Table S2: Selected bond lengths (Å) and angles (°) of crystal structure of **5**; Table S3: TDDFT results (excitation wavelengths [nm], oscillator strengths [*f*], and major contributions) of **4**. Here, transitions with oscillator strengths greater than 0.002 and excitation contributions exceeding 10% were selected; Table S4: TDDFT results (excitation wavelengths [nm], oscillator strengths [*f*], and major contributions) of **5**. Here, transitions with oscillator strengths greater than 0.002 and excitation contributions exceeding 10% were selected.

**Author Contributions:** Conceptualization, Y.K.; methodology, Y.K.; validation, N.Y., M.H. and Y.K.; formal analysis, N.T., N.Y., M.H. and Y.K.; investigation, N.T. and Y.K.; resources, Y.K.; data curation, Y.K.; writing—original draft preparation, Y.K.; writing—review and editing, N.T., N.Y., M.H. and Y.K.; visualization, Y.K.; supervision, Y.K.; project administration, Y.K.; funding acquisition, N.Y., M.H. and Y.K. All authors have read and agreed to the published version of the manuscript.

**Funding:** This research was supported by JSPS KAKENHI (grant numbers JP24K08494, JP24K08363, and JP25K18113).

**Data Availability Statement:** The original contributions presented in this study are included in the article/supplementary material. Further inquiries can be directed to the corresponding authors.

**Acknowledgments:** A part of this work was conducted at the Institute for Molecular Science, which was supported by "Advanced Research Infrastructure for Materials and Nanotechnology in Japan (ARIM)" of the Ministry of Education, Culture, Sports, Science and Technology (MEXT) (Proposal Number JPMXP1225MS1036).

**Conflicts of Interest:** The authors declare no conflicts of interest.

## References

1. Cotton, F.A.; Murillo, C.A.; Walton, R.A. *Multiple Bonds Between Metal Atoms*, 3rd ed.; Springer Science and Business Media: New York, NY, USA, 2005.
2. Cotton, F.A.; Lin, C.; Murillo, C.A. Supramolecular Arrays Based on Dimetal Building Units. *Acc. Chem. Res.* **2001**, *34*, 759–771. [CrossRef]
3. Chisholm, M.H.; Patmore, N.J. Studies of Electronic Coupling and Mixed Valency in Metal-Metal Quadruply Bonded Complexes Linked by Dicarboxylate and Closely Related Ligands. *Acc. Chem. Res.* **2007**, *40*, 19–27. [CrossRef]

4. Aquino, M.A.S. Diruthenium and diosmium tetracarboxylates: Synthesis, physical properties, and applications. *Coord. Chem. Rev.* **1998**, *170*, 141–202. [CrossRef]
5. Van Caemelbecke, E.; Phan, T.; Osterloh, W.R.; Kadish, K.M. Electrochemistry of metal-metal bonded diruthenium complexes. *Coord. Chem. Rev.* **2021**, *434*, 213706. [CrossRef]
6. Cortijo, M.; González-Prieto, R.; Herrero, S.; Priego, J.L.; Jiménez-Aparicio, R. The use of amidinate ligands in paddlewheel diruthenium chemistry. *Coord. Chem. Rev.* **2019**, *400*, 213040. [CrossRef]
7. Kataoka, Y.; Yano, N.; Mikuriya, M.; Handa, M. Coordination polymers and metal–organic frameworks based on paddlewheel-type dirhodium(II) tetracarboxylates. *Coord. Chem. Rev.* **2022**, *472*, 214796. [CrossRef]
8. Kataoka, Y.; Yano, N.; Mikuriya, M.; Handa, M. Paddlewheel-type dirhodium complexes with N,N′-bridging ligands. *Coord. Chem. Rev.* **2023**, *479*, 214997. [CrossRef]
9. Ren, T. Substituent effects in dinuclear paddlewheel compounds: Electrochemical and spectroscopic investigations. *Coord. Chem. Rev.* **1998**, *175*, 43–58. [CrossRef]
10. Aquino, M.A.S. Recent developments in the synthesis and properties of diruthenium tetracarboxylates. *Coord. Chem. Rev.* **2004**, *248*, 1025–1045. [CrossRef]
11. Miyasaka, H. Charge Manipulation in Metal-Organic Frameworks: Toward Designer Functional Molecular Materials. *Bull. Chem. Soc. Jpn.* **2021**, *94*, 2929–2955. [CrossRef]
12. Hansen, J.; Davies, H.M.L. High symmetry dirhodium(II) paddlewheel complexes as chiral catalysts. *Coord. Chem. Rev.* **2008**, *252*, 545–555. [CrossRef]
13. Fiori, K.W.; Du Bois, J. Catalytic Intermolecular Amination of C−H Bonds: Method Development and Mechanistic Insights. *J. Am. Chem. Soc.* **2007**, *129*, 562–568. [CrossRef] [PubMed]
14. Chifotides, H.T.; Dunbar, K.R. Interactions of Metal−Metal-Bonded Antitumor Active Complexes with DNA Fragments and DNA. *Acc. Chem. Res.* **2005**, *38*, 146–156. [CrossRef]
15. Uemura, K. One-dimensional complexes extended by unbridged metal–metal bonds based on a HOMO–LUMO interaction at the $dz^2$ orbital between platinum and heterometal atoms. *Dalton Trans.* **2017**, *46*, 5474–5492. [CrossRef]
16. Knöfel, N.D.; Schoo, C.; Seifert, T.P.; Roesky, P.W. A dimolybdenum paddlewheel as a building block for heteromultimetallic structures. *Dalton Trans.* **2020**, *49*, 1513–1521. [CrossRef] [PubMed]
17. Mori, W.; Sato, T.; Nozaki Kato, C.; Takei, T.; Ohmura, T. Discovery and development of microporous metal carboxylates. *Chem. Rec.* **2005**, *5*, 336–351. [CrossRef]
18. Chipman, J.A.; Berry, J.F. Paramagnetic Metal–Metal Bonded Heterometallic Complexes. *Chem. Rev.* **2020**, *120*, 2409–2447. [CrossRef]
19. Liao, Y.; Shum, W.W.; Miller, J.S. Synthesis and Magnetic Properties of 3-D $[Ru^{II/III}{}_2(O_2CMe)_4]_3[M^{III}(CN)_6]$ (M = Cr, Fe, Co). *J. Am. Chem. Soc.* **2002**, *124*, 9336–9337. [CrossRef]
20. Mikuriya, M.; Yoshioka, D.; Handa, M. Magnetic interactions in one-, two-, and three-dimensional assemblies of dinuclear ruthenium carboxylates. *Coord. Chem. Rev.* **2006**, *250*, 2194–2211. [CrossRef]
21. Miyasaka, H.; Motokawa, N.; Matsunaga, S.; Yamashita, M.; Sugimoto, K.; Mori, T.; Toyota, N.; Dunbar, K.R. Control of Charge Transfer in a Series of $Ru_2{}^{2+}$/TCNQ Two-Dimensional Networks by Tuning the Electron Affinity of TCNQ Units: A Route to Synergistic Magnetic/Conducting Materials. *J. Am. Chem. Soc.* **2010**, *132*, 1532–1544. [CrossRef]
22. Liu, B.; Jin, J.; Liu, X.-M.; Hu, H.-M.; Ding, T.; Zhang, N.; Jia, Y.-Y.; Xue, G.-L. A diruthenium soft ferromagnet showing $T_c$ = 3.0 K: $Mn_4(H_2O)_{16}H[Ru_2(CO_3)_4]_2[Ru_2(CO_3)_4(H_2O)_2]\cdot 11H_2O$. *Dalton Trans.* **2012**, *41*, 4748–4750. [CrossRef] [PubMed]
23. Trenerry, M.J.; Wallen, C.M.; Brown, T.R.; Park, S.V.; Berry, J.F. Spontaneous $N_2$ formation by a diruthenium complex enables electrocatalytic and aerobic oxidation of ammonia. *Nat. Chem.* **2021**, *13*, 1221–1227. [CrossRef]
24. Kataoka, Y.; Sato, K.; Miyazaki, Y.; Masuda, K.; Tanaka, H.; Naito, S.; Mori, W. Photocatalytic hydrogen production from water using porous material $[Ru_2(p\text{-}BDC)_2]_n$. *Energy Environ. Sci.* **2009**, *2*, 397–400. [CrossRef]
25. Villalobos, L.; Barker Paredes, J.E.; Cao, Z.; Ren, T. *tert*-Butyl Hydroperoxide Oxygenation of Organic Sulfides Catalyzed by Diruthenium(II,III) Tetracarboxylates. *Inorg. Chem.* **2013**, *52*, 12545–12552. [CrossRef] [PubMed]
26. Miyazawa, T.; Suzuki, T.; Kumagai, Y.; Takizawa, K.; Kikuchi, T.; Kato, S.; Onoda, A.; Hayashi, T.; Kamei, Y.; Kamiyama, F.; et al. Chiral paddle-wheel diruthenium complexes for asymmetric catalysis. *Nat. Catal.* **2020**, *3*, 851–858. [CrossRef]
27. Tolbatov, I.; Barresi, E.; Taliani, S.; La Mendola, D.; Marzo, T.; Marrone, A. diruthenium(II,III) paddlewheel complexes: Effects of bridging and axial ligands on anticancer properties. *Inorg. Chem. Front.* **2023**, *10*, 2226–2238. [CrossRef]
28. Terán, A.; Ferraro, G.; Sánchez-Peláez, A.E.; Herrero, S.; Merlino, A. Effect of Equatorial Ligand Substitution on the Reactivity with Proteins of Paddlewheel Diruthenium Complexes: Structural Studies. *Inorg. Chem.* **2023**, *62*, 670–674. [CrossRef] [PubMed]

29. Kataoka, Y.; Imasaki, N.; Yano, N.; Mitsumi, M.; Handa, M. Redox-triggered reversible modulation of intense near-infrared and visible absorption using paddlewheel-Type diruthenium(III) complex. *Dalton Trans.* **2021**, *50*, 9547–9553. [CrossRef]
30. Lindsay, A.J.; Wilkinson, G.; Motevalli, M.; Hursthouse, M.B. The synthesis, magnetic, electrochemical, and spectroscopic properties of diruthenium(II,II) tetra-μ-carboxylates and their adducts. X-ray Structures of $Ru_2(O_2CR)_4L_2$ (R = Me, L = $H_2O$ or Tetrahydrofuran; R = Et, L = $Me_2CO$). *J. Chem. Soc. Dalton Trans.* **1985**, *11*, 2321–2326. [CrossRef]
31. Furukawa, S.; Kitagawa, S. Neutral Paddlewheel Diruthenium Complexes with Tetracarboxylates of Large π-Conjugated Substituents: Facile One-Pot Synthesis, Crystal Structures, and Electrochemical Studies. *Inorg. Chem.* **2004**, *43*, 6464–6472. [CrossRef]
32. Kataoka, Y.; Tada, N.; Masamori, N.; Yano, N.; Moriyoshi, C.; Handa, M. Paddlewheel-type and half-paddlewheel-type diruthenium(II,II) complexes with 1,8-naphthyridine-2-carboxylate. *Dalton Trans.* **2025**, *54*, 3047–3056. [CrossRef]
33. Kataoka, Y.; Tada, N.; Omaki, J.; Matsubara, K.; Yano, N.; Handa, M. Paddlewheel-Type Diruthenium(II) Naphthyridine Complex with Electron-Withdrawing Trifluoroacetate Ligands. *Chemistry* **2025**, *7*, 72. [CrossRef]
34. Tada, N.; Yano, N.; Mizogami, Y.; Matsubara, K.; Handa, M.; Kataoka, Y. Paddlewheel-Type Diruthenium(II,II) Naphthyridine Complexes with π-Conjugated Aromatic Carboxylate Ligands. *Cryst. Growth Des.* **2025**, *25*, 4458–4465. [CrossRef]
35. Miyasaka, H.; Motokawa, N.; Atsuumi, R.; Kamo, H.; Asai, Y.; Yamashita, M. Tuning of the ionization potential of paddlewheel diruthenium(II,II) complexes with fluorine atoms on the benzoate ligands. *Dalton Trans.* **2011**, *40*, 673–682. [CrossRef]
36. Kosaka, W.; Watanabe, Y.; Aliyah, K.H.; Miyasaka, H. Role of intramolecular hydrogen bonding in the redox chemistry of hydroxybenzoate-bridged paddlewheel diruthenium(II,II) complexes. *Dalton Trans.* **2022**, *51*, 85–94. [CrossRef]
37. Delgado-Martínez, P.; Elvira-Bravo, A.; González-Prieto, R.; Priego, J.L.; Jimenez-Aparicio, R.; Torres, M.R. Synthesis of $Ru_2Br(\mu\text{-}O_2CC_6H_4\text{–}R)_4$ (*R* = *o*-Me, *m*-Me, *p*-Me) Using Microwave Activation: Structural and Magnetic Properties. *Inorganics* **2014**, *2*, 524–536. [CrossRef]
38. *CrysAlisPro*, version 1.171.43.108a; Rigaku Oxford Diffraction: Oxford, UK, 2018.
39. Sheldrick, G.M. *SHELXT*—Integrated space-group and crystal-structure determination. *Acta Cryst.* **2015**, *A71*, 3–8. [CrossRef] [PubMed]
40. Sheldrick, G.M. Crystal structure refinement with *SHELXL*. *Acta Cryst.* **2015**, *C71*, 3–8.
41. Dolomanov, O.V.; Bourhis, L.J.; Gildea, R.J.; Howard, J.A.K.; Puschmann, H. OLEX2: A complete structure solution, refinement and analysis program. *J. Appl. Cryst.* **2009**, *42*, 339–341. [CrossRef]
42. Becke, A.D. Density–functional thermochemistry. III. The role of exact exchange. *J. Chem. Phys.* **1993**, *98*, 5648–5652. [CrossRef]
43. Andrae, D.; Haeussermann, U.; Dolg, M.; Stoll, H.; Preuss, H. Energy-adjusted *ab* initio pseudopotentials for the second and third row transition elements. *Theor. Chem. Acc.* **1990**, *77*, 123–141. [CrossRef]
44. Dunning, T.H., Jr. Gaussian basis sets for use in correlated molecular calculations. I. The atoms boron through neon and hydrogen. *J. Chem. Phys.* **1989**, *90*, 1007–1023. [CrossRef]
45. Frisch, M.J.; Trucks, G.W.; Schlegel, H.B.; Scuseria, G.E.; Robb, M.A.; Cheeseman, J.R.; Scalmani, G.; Barone, V.; Petersson, G.A.; Nakatsuji, H.; et al. *Gaussian 16, Revision C.01*; Gaussian, Inc.: Wallingford, CT, USA, 2016.
46. Tomasi, J.; Mennucci, B.; Cammi, R. Quantum Mechanical Continuum Solvation Models. *Chem. Rev.* **2005**, *105*, 2999–3093. [CrossRef] [PubMed]
47. Adamo, C.; Jacquemin, D. The calculations of excited-state properties with time-dependent density functional theory. *Chem. Soc. Rev.* **2013**, *42*, 845–856. [CrossRef] [PubMed]
48. Campos-Fernández, C.S.; Thomson, L.M.; Galán-Mascarós, J.R.; Ouyang, X.; Dunbar, K.R. Homologous Series of Redox-Active, Dinuclear Cations $[M_2(O_2CCH_3)_2(pynp)_2]^{2+}$ (M = Mo, Ru, Rh) with the Bridging Ligand 2-(2-Pyridyl)-1,8-naphthyridine (pynp). *Inorg. Chem.* **2002**, *41*, 1523–1533. [CrossRef]
49. Sharma, R.P.; Kumar, S.; Venugopalan, P.; Ferretti, V.; Tarushi, A.; Psomas, G.; Witwicki, M. New copper(II) complexes of the anti-inflammatory drug mefenamic acid: A concerted study including synthesis, physicochemical characterization and their biological evaluation. *RSC Adv.* **2016**, *6*, 88546–88558. [CrossRef]
50. Miyasaka, H.; Clérac, R.; Campos-Fernández, C.S.; Dunbar, K.R. The first crystal structure of a one-dimensional chain of linked $Ru^{II}$–$Ru^{II}$ units. *J. Chem. Soc. Dalton Trans.* **2001**, 858–861. [CrossRef]
51. Chen, W.-Z.; Cotton, F.A.; Dalal, N.S.; Murillo, C.A.; Ramsey, C.M.; Ren, T.; Wang, X. Proof of Large Positive Zero-Field Splitting in a $Ru_2^{5+}$ Paddlewheel. *J. Am. Chem. Soc.* **2005**, *127*, 12691–12696. [CrossRef]
52. Shum, W.W.; Liao, Y.; Miller, J.S. Zero-Field Splitting, Field-Dependent Magnetization of Mixed-Valent *S* = 3/2 Diruthenium(II,III) Tetracarboxylates. *J. Phys. Chem. A* **2004**, *108*, 7460–7462. [CrossRef]
53. Cotton, F.A.; Miskowski, V.M.; Zhong, B. Chemistry, Structure and Bonding in Diruthenium(II) Tetracarboxylates. *J. Am. Chem. Soc.* **1989**, *111*, 6177–6182. [CrossRef]

54. Cotton, F.A.; Ren, T.; Eglin, J.L. Further Investigation of Molecular, Magnetic, and Electronic Structures of 2-Hydroxypyridinate Complexes of Diruthenium(II). *Inorg. Chem.* **1991**, *30*, 2552–2558. [CrossRef]
55. Cukiernik, F.D.; Giroud-Godquin, A.-M.; Maldivi, P.; Marchon, J.-C. Pyrazine-mediated antiferromagnetic intermolecular exchange in mixed-valent diruthenium tetracarboxylates. *Inorg. Chim. Acta* **1994**, *215*, 203–207. [CrossRef]